Efficient Heating at the Third-Harmonic Electron Cyclotron Resonance in the Large Helical Device

Takashi SHIMOZUMA, Shin KUBO, Hiroe IGAMI, Yasuo YOSHIMURA, Takashi NOTAKE[1],
Nikolai B. MARUSHCHENKO[2], Yurij TURKIN[2], Takashi MUTOH
and the LHD Experimental Group

National Institute for Fusion Science, 322-6 Oroshi-cho, Toki 509-5292, Japan
[1]*University of Fukui, Research Center for Development of Far-Infrared Region, 3-9-1 Bunkyo, Fukui 910-8507, Japan*
[2]*Max-Plank-Institut für Plasmaphysik, EURATOM-Association, Wendelsteinstr. 1, D-17491 Greifswald, Germany*

Efficient heating at the third-harmonic electron cyclotron resonance was attained by injection of millimeter-wave power with 84 GHz frequency range at the magnetic field strength of 1 T in LHD. The electron temperature at the plasma center clearly increased, and the increment in the temperature reached 0.2-0.3 keV. The dependence of the power absorption rate on the antenna focal position was investigated experimentally, showing that the optimum position was located in the slightly high-field side of the resonance layer. Ray-tracing calculation was performed in the realistic three-dimensional magnetic configuration, and its results are compared with the experimental results.

1. Introduction

High-harmonic heating of the electron cyclotron resonance (ECR) is an attractive method to extend the heating regime of plasma parameters by alleviating the density limitation due to some cutoffs of EC wave propagation. In the LHD launching geometry, the magnetic field strength is almost constant along the ray paths launched from upper- and lower-port antennas, which cross near the magnetic axis. Under this condition, the ray can remain resonant with electrons over a considerable length. Therefore, good absorption is expected over a wide density range even for the third-harmonic resonance heating by the linear theory [1].

Third harmonic resonance heating was attempted experimentally in Heliotron DR and effective heating was observed [2]. In TCV tokamak, third harmonic resonance heating was performed with second-harmonic resonance heating using gyrotrons of two different frequencies such as 82.7 GHz for the second harmonic and 118 GHz for the third harmonic resonance. Hundred percent absorption was attained on the existence of high energy electrons produced by the second-harmonic resonance heating [3,4]. Further, a sophisticated feedback control of antenna focal position realized 100 % absorption by only third-harmonic resonance heating [5]. In W7-X, third-harmonic heating is planned as a candidate of a normal heating scenario in the high density regime (0.6-2.0 × 10²⁰ m⁻³) using a 140 GHz,

10 MW ECH system [6].

Effective third-harmonic resonance heating has already been achieved in the 2 T LHD plasma by injection of 168 GHz millimeter-wave power from upper-port antennas. In the experiments of third-harmonic resonance heating, obvious heating of the bulk plasma ($\Delta T_e = 0.2$ keV) around the plasma center by 340 kW power injection was observed [7].

Because the ECH power in the 84 GHz range has recently been upgraded up to 1.3 MW, we attempted third harmonic extraordinary(X)-mode heating by injection of 84 GHz range power at the magnetic field strength of 1 T with a magnetic axis of 3.75 m. When the same frequency is used, the cutoff density for the third harmonic X-mode heating at 1 T becomes 4/3 times higher than that for second harmonic X-mode heating at 1.5 T. It is about 6×10^{19} m⁻³.

2. Experimental Setup and Results

The ECH system consists of 84 GHz range and 168 GHz gyrotrons, high-voltage power supplies, long distance transmission lines, and in-vessel quasi-optical antennas. It has been improved step by step. At the last campaign(2006) of LHD experiments, five 84 GHz range and three 168 GHz gyrotrons were operated, and ECH power could be injected from six antennas in the vertically elongated cross-section (upper-port and lower-port antennas) and two antennas in the horizontally elongated cross-

Fig. 1   Wave form of NBI power, ECH timing, stored energy W_p, and line-averaged density from top to bottom.
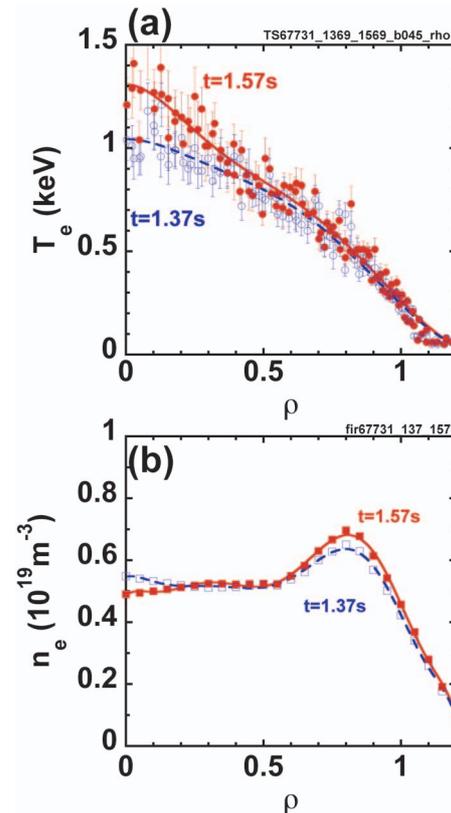

Fig. 2   Profiles of electron temperature in (a) and electron density in (b) just before ($t = 1.37$ sec: open symbols) and during ($t = 1.57$ sec: closed symbols) ECH are plotted. ρ is the normalized minor radius.

section (outer-port antennas).

Two kinds of antenna systems for ECH are installed in the LHD vacuum vessel. The vertical injection antenna system consists of two or four millimeter-wave focusing and steering mirrors. The high power measurement of this system shows good agreement with the designed beam-waist size of 15 mm in radial and 50 mm in toroidal directions for the upper-port antennas and of 30 mm for the lower-port antennas. The direction of the beam can be steered radially and toroidally, respectively. The injected millimeter-wave beams from these antennas consequently have a grazing incidence angle to the cyclotron resonance and continue to interact along a long ray-path. For horizontal injection, the antenna system consists of two mirrors, one is fixed and another is steerable. The movable range covers the whole plasma cross-section for perpendicular injection and can be changed over a range of about ±30 degrees toroidally. In this case, the injected beams perpendicularly pass through the ECR layer with the shortest gradient length. A magnetic configuration was chosen such that the third-harmonic ECR was located near the magnetic axis for both the vertically and horizontally elongated cross-sections, because the microwave beams from all antennas could access almost perpendicular to the magnetic field line of force. Therefore, the magnetic field strength of 1 T on the magnetic axis placed on $R = 3.75$ m was adopted without plasmas.

In the experiments, target plasmas were produced and sustained by only NBI power. The electron temperature of a target plasma was about 1 keV and the line-averaged density was 0.6×10^{19} m^{-3} at the center. ECH power (1.3 MW) was injected from $t = 1.4$ sec and 1.5 sec in a stair-like manner, as shown in Fig. 1. The ECH pulse, which has a longer pulse width, corresponds to 84 GHz power from the outer-port antenna. The ECH pulse with a shorter pulse width is 82.7 GHz from upper-port antennas and 84 GHz from lower-port antennas. The absorption rate for the different types of resonance can be discriminated independently and effectively by the stair-like injection. An obvious increase in the stored energy was observed during both the first and second ECH pulses, while there was no change in the density. Figure 2 shows the profiles of electron temperature measured by Thomson scattering and electron density measured by a far-infrared laser (FIR) interferometer just before ($t = 1.37$ sec) and during ($t = 1.57$ sec) ECH power injection. The plasma center was heated efficiently, and the increment in the temperature reached 0.2-0.3 keV. The electron density profile was rather hollow both before and during the ECH pulse. Density pump-out is noticed around the center during ECH ($t = 1.57$ sec).

Absorbed power was estimated using the increment in the plasma stored energy dW_p/dt before and after ECH on-times, assuming that the other plasma parameters did not change quickly. The dependences on the focal point R_{foc} of the upper-port antennas (82.7 GHz) and on line-averaged density were examined and shown in Fig. 3 (a) and (b), respectively. In Fig. 3 (a), closed circles denote experimentally obtained data for the line-averaged electron density of about 0.6×10^{19} m^{-3}. The maximum absorption rate was obtained on the antenna focal position $R_{foc} = 3.7$ m, which was smaller than the third harmonic ECR
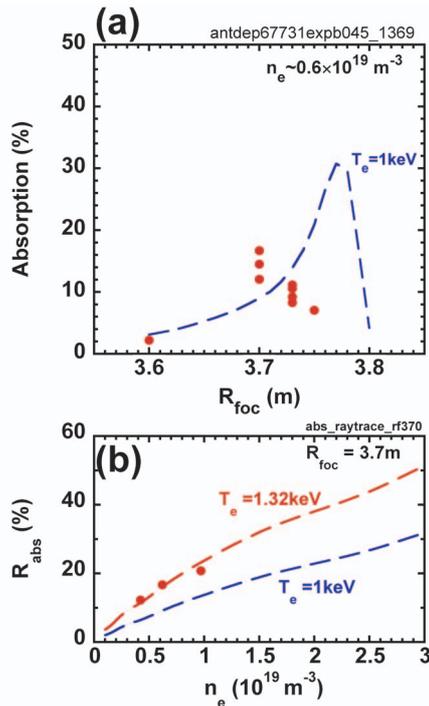
Fig. 3 Efficiency of absorbed power for the 82.7 GHz antenna was estimated by change in dW_p/dt at ECH on-time. Antenna focal point on the equatorial plane R_{foc} dependence is shown by closed circles for the density of $0.6 \times 10^{19} m^{-3}$ in (a). Electron density dependence is also shown for $R_{foc} = 3.7$ m in (b). The calculation results obtained by ray-tracing are also plotted by dashed lines with an assumed electron temperature.

Fig. 4 Single-pass absorption rate for injection from the upper-port antenna is contour-plotted in the electron temperature and density space. The focal point corresponds to $R_{foc} = 3.7$ m. The profiles of the temperature and density are assumed to be those shown in Fig. 2. Contour lines of absorption rate are drawn at intervals of 0.1.
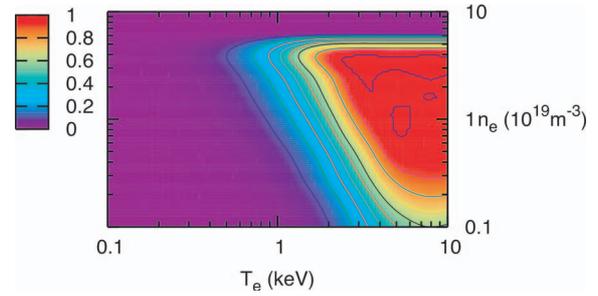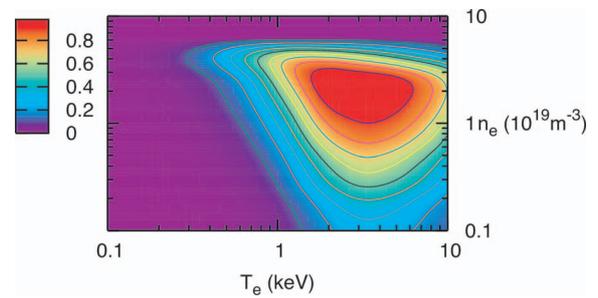

Fig. 5 Single-pass absorption rate for injection from the upper-port antenna is contour-plotted in the electron temperature and density space. The focal point corresponds to $R_{foc} = 3.75$ m. The profiles of the temperature and density are assumed to be those shown in Fig. 2. Contour lines of absorption rate are drawn at intervals of 0.1.

layer (3.78 m). The absorption rate, however, is rather low, because the temperature and density of the target plasma was fairly low. The density dependence of the absorption rate is plotted for $R_{foc} = 3.7$ m in Fig. 3 (b). In these figures, dashed lines represent the results of ray-tracing calculations. In the calculations, the dispersion relation of a cold plasma was assumed for ray-trajectory calculations, and the weakly relativistic effect was included for the absorption calculations [8]. The polynomial fitted data of electron temperature and density profiles shown in Fig. 2 were used. There is a great difference between experimental data and ray-tracing calculations in the focal position dependence. The calculation results reflect strong single-pass absorption around ECR corresponding to $R \simeq 3.78$ m. The maximum value reaches about 30%. The gradual decrease at $R_{foc} > 3.7$ m noticed in the experimental data cannot be explained by expectations of ray-tracing. On the other hand, the density dependence of the absorption agreed well with the calculation for $T_e \simeq 1.3$ keV. The experimental results show efficient heating up to $R_{abs} \simeq 20\%$ at the third-harmonic resonance even for the fairly low electron temperature (~ 1 keV) and low electron density ($\sim 1 \times 10^{19}$ m^{-3}).

In order to examine the dependence of the single-pass absorption rate on the electron temperature T_e and density n_e, ray-tracing calculation was performed expensively over two orders of magnitude in the $T_e - n_e$ space. The experimentally obtained profiles shown in Fig. 2 were used in the calculations. Because the optical thickness scales as $\tau \sim n_e \cdot T_e^2$, a little temperature change possibly leads to fairly large difference in the absorption rate. Figure 4 shows a contour-plot of the single-pass absorption rate in the electron temperature and density space for the injection from the upper-port antenna with $R_{foc} = 3.7$ m. The values of temperature, T_e, and density, n_e, in the figure represent the values at the center. The figure clearly shows that almost 100 % absorption is expected in the high-temperature ($\gtrsim 3$ keV) high-density ($1\text{-}4 \times 10^{19}$ m^{-3}) region up to the right-hand cut-off density. However, in the low-temperature ($\lesssim 1$ keV) low-density ($\lesssim 1 \times 10^{19}$ m^{-3}) region, the absorption rate can change from several percent to several tens of percent according to the small change in plasma parameters around the resonance layer.

This mapping of the absorption rate is strongly affected by the focal point of the injection beam as expected. Figure 5 shows the same $T_e - n_e$ mapping of single-pass absorption for $R_{foc} = 3.75$ m. It is obvious that the high ef-

ficiency region moves to a lower-temperature area, because the relativistic down-shift of ECR leads to father off-axis heating. This clearly indicates that the temperature at the beam focal point is more important than its profile.

3. Comparative Study with Ray-Tracing Calculations by TRAVIS code in LHD magnetic Configuration

A more sophisticated ray-tracing code, "TRAVIS" was used to study some effects, such as relativistic and anomalous dispersion effects on ray trajectories and the existence of trapped particles on the absorption rate, for experimentally obtained electron temperature and density profiles in the LHD magnetic field configuration.

The ray-tracing code, "TRAVIS (IPP)", has been developed for ECH/ECCD and ECE studies in an arbitrary three-dimensional magnetic configuration [9, 10]. The basic ray-tracing equations include weakly relativistic formulation for Hamiltonian, taking into account possible anomalous dispersion effects. The Gaussian power distribution of an injected beam is assumed and the beam cross-section is discretized by the arbitrary number of radial and azimuthal points. Wave absorption can be calculated in a fully relativistic formulation. Power deposition is decomposed to passing and trapped electron contributions. Extraordinary-mode waves are assumed to be injected from the upper-port antenna with a frequency of 82.7 GHz and the lower-port antenna with 84 GHz focused around the magnetic axis. In these calculations, the experimentally obtained electron temperature and density profiles which are shown in Fig. 2 at 1.37 s, were used. In Fig. 6, the configuration of the calculation is illustrated with mod-B contours, flux surfaces with a plasma β value of 0.33 %, and wave rays. The third harmonic ECR is also depicted. Typical calculated ray trajectories from the upper-port antenna in Fig. 6 (a) and lower-port antenna in (b) are shown. No relativistic or anomalous effects were found in the trajectories in such a low temperature low-density plasma, and the trajectories follow almost straight-line paths.

The same focal point dependence of the absorption rate was investigated using the TRAVIS code. The result in Fig. 7 shows that almost equal values and dependence was reproduced with the same plasma parameters, when compared with the dashed line in Fig. 3 (a). This fact also implies that the relativistic and anomalous effects are weak in these parameter regimes.

Figure 8 shows the profiles of the absorbed power density in (a) and the integrated absorbed power in (b) for 84 GHz wave injected from the lower-port antenna, which corresponds to Fig. 6 (b). The absorption occurred along the third-harmonic resonance line (B = 1 T) and the deposition spreads over from $\rho \sim 0.1$ to 0.6, as shown in
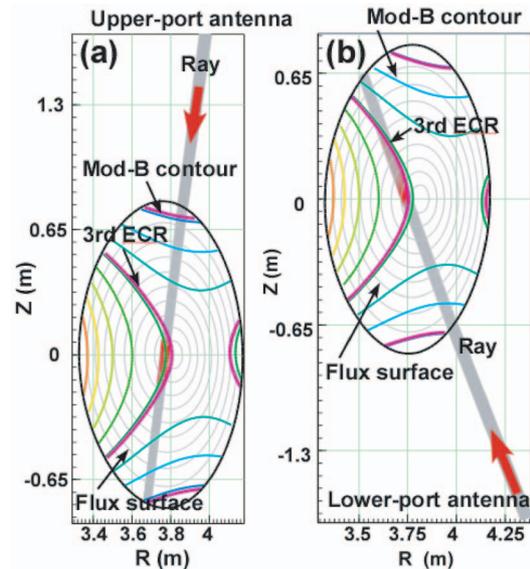

Fig. 6 Ray tracing calculation together with ECR, mod-B contours and flux surfaces. (a) Upper-port antenna injection. (b) Lower-port antenna injection. The strongly absorbed regions are indicated by red color around the high-field-side of third-harmonic ECR.
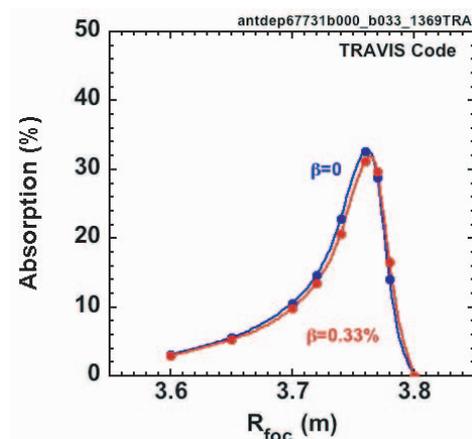

Fig. 7 Focal point dependence of single-pass absorption calculated by TRAVIS for 82.7 GHz waves injected from the upper-port antenna.

Fig. 8 (a). Most of the power is absorbed by the passing electrons near the magnetic axis, because the helical ripples there are small in this magnetic configuration. On the other hand, the fraction of absorption by trapped particles becomes dominant toward the plasma periphery $\rho \sim 0.3$-0.5, where the helical ripples increase. Maximum absorption rate is about 28.4 %. This value is somewhat larger than the experimental one. One of the possible reasons is the production of supra-thermal electrons by the third-harmonic ECR, which could be drifting out from a plasma quickly before thermalization, and do not contribute to the increment in diamagnetic energy of the plasma. This fact can partly explain the discrepancy between the values of the single-pass absorption calculated by ray-tracing and
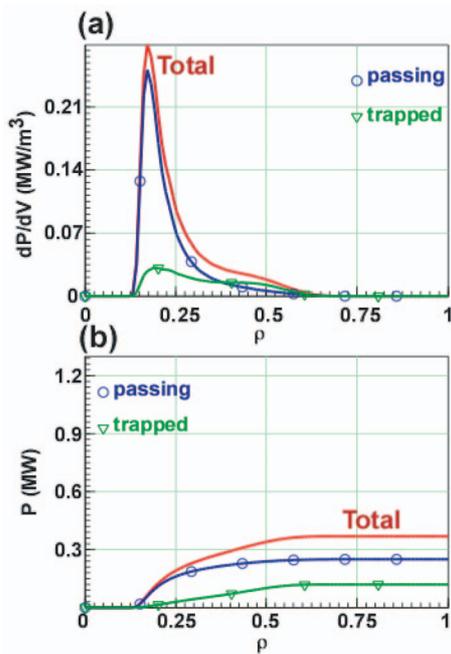
Fig. 8 Power deposition. (a) Deposited power density is plotted as a function of normalized minor radius and (b) integral value of absorbed power along the ray path. Total amount is decomposed into each component absorbed by passing and trapped electrons.

the absorption rate evaluated from the temporal change of dW_p/dt.

4. Summary

Third harmonic ECR heating experiments were performed. In particular, because of the upgrade of 84 GHz gyrotrons and the transmission line, efficient heating results were obtained even for the third-harmonic resonance. During the ECH pulse of 0.4 sec, the stored energy of the plasma increased by several percents. The central electron temperature increased by about 0.2-0.3 keV. The dependence of the absorption rate on the antenna focal position shows the maximum at a slightly higher-field side of the resonance position.

In order to discuss a detailed quantitative comparison, ray-tracing calculation was performed and compared with experimental data. The calculation was based on the assumption of a cold plasma dispersion relation for trajectory calculation and of the weakly relativistic effect for absorption. The results imply that the absorption rate strongly depends on the values of the electron temperature and density themselves, in the area where the wave is absorbed, and not on the profile in this plasma parameter region. The experimentally evaluated absorption rate for R_{foc} = 3.7 m shows fairly good agreement with the results of the ray-tracing calculation. Nonetheless, the cal-

culation cannot completely explain the behavior on focal point dependence. Because the errors of the focal position setting of each antenna, which are about 1-3 cm, cannot explain the discrepancy, supra-thermal electrons produced by the third harmonic resonance and their quick escape from plasma core possibly play a role in suppressing the increase in the stored energy.

More sophisticated calculation using ray-tracing code "TRAVIS", which has been developed in IPP Greifswald (Germany), was successfully performed in the three-dimensional magnetic configuration of LHD. In this code, relativistic and anomalous dispersion effects on ray trajectories and the existence of trapped particles on the absorption rate are taken into account. The results of calculation performed in the LHD magnetic configuration and the actual temperature and density profiles show no relativistic and anomalous effects in this plasma parameter regime. The contribution of trapped particles to the absorption reaches about one-third of the total absorption. This partly explains the smaller efficiency in experimental results compared with the calculated efficiency. The experiments discriminating the contribution of trapped particles should be performed by changing the magnetic configuration. These issues will be dealt with in future.

Acknowledgment

[1] U. Gasparino, H. Idei, S. Kubo et al., Nucl. Fusion 38, 223 (1998).
[2] N. Yanagi, S. Morimoto, M. Sato et al., Nucl. Fusion 31, 261 (1991).
[3] S. Alberti, T.P. Goodman, M.A. Henderson et al., Nucl. Fusion 42, 42 (2002).
[4] G. Arnoux et al., Plasma Phys. Control. Fusion 47, 295 (2005).
[5] S. Alberti et al., Nucl. Fusion 45, 1224 (2005).
[6] H.P. Laqua, V. Erckmann, R. Brakel et al., 15th International Stellarator Workshop, Madrid,3-7, October 2005, IT-20.
[7] T. Shimozuma, H. Idei et al., 27th European Physical Society Conference on Controlled Fusion and Plasma Physics, Budapest, Hungary, June 12-16, 2000, P4.019.
[8] S. Kubo, T. Shimozuma et al., Plasma Phys. Control. Fusion 47, A81 (2005).
[9] N.B. Marushchenko, V. Erckmann, H. Maaßberg, Yu. Turkin, 34th European Physical Society Conference on Plasma Physics, Warsaw, Poland, July 2-6, 2007, P5.129.
[10] N.B. Marushchenko et al., Plasma Fusion Res. 2, S1129 (2007).